Soil Moisture Retrieval Using L-Band Radar Observations

Parag S. Narvekar, *Member, IEEE*, Dara Entekhabi, *Senior Member, IEEE*, Seung-Bum Kim, and Eni G. Njoku, *Fellow, IEEE*

***Abstract*—An algorithm for surface soil moisture estimation using L-band radar observations is introduced. The formulation envelops a wide range of land surface conditions based on three limiting cases defined in terms of end-members: smooth bare soil, rough bare soil, and a maximum vegetation covered soil. Parameterizations for these end-members are obtained using forward electromagnetic scattering models. Modulation due to soil surface roughness and overlying vegetation scattering effects between end-members are accounted using the radar vegetation index and the newly introduced radar roughness index. Hence, the retrieval algorithm developed here does not depend on ancillary vegetation or roughness information. The algorithm is tested with ground-based truck-mounted bare soil observations and observations from several airborne field campaigns that represent a wide range of surface conditions.**

***Index Terms*—Radar roughness (RR), radar soil moisture, radar vegetation.**

I. Introduction

THE microwave remote sensing of the Earth surface and specifically the retrieval of surface soil moisture content performed with passive sensors have been demonstrated to be more robust than those performed with active sensors. The scattering and attenuation due to the vegetation cover and surface roughness effects strongly influence the active signal when compared to the passive signal. However, the lower spatial resolutions of spaceborne passive sensors limit their applicability to many applications. Active sensors like spaceborne radars provide observations at higher spatial resolutions. However, difficulties in quantifying scattering effects pose challenges for soil moisture estimation using active measurements. In this paper, we develop a robust radar-only soil moisture algorithm. The algorithm is designed to work with L-band radar measurements.

In order to make the algorithm computationally efficient for soil moisture estimation, all possible efforts are made to keep the formulation independent of the ancillary information source on vegetation and surface roughness. Furthermore, ancillary information on vegetation and roughness often depends on empirical parameterizations using optical sensor data (e.g., vegetation indices and land-use classification). The ancillary information is itself a source of error. The proposed algorithm is applicable with the sensing configuration of the upcoming Soil Moisture Active Passive (SMAP) mission [1].

A major challenge in accurately retrieving soil moisture from spaceborne radar observations is that the number of observations from a particular radar sensor is less than the unknown surface parameters. These parameters include multiple scales of roughness and potentially several vegetation characteristics. In order to address these issues, several approaches have been developed using a combination of theory and empiricism based on ground-based, airborne, and spaceborne radar observations, e.g., [2]–[8]. In these approaches, assumptions are made regarding scattering from different vegetation components and from different scaled surface roughness. One assumption that is usually made to overcome the difficulty in adequately accounting for the scattering effect from vegetation is to treat vegetation as a uniform medium of some specified height with randomly oriented scatterers [2], [9], [10]. However, these theoretical representations can be ill-posed inverse problems due to the large number of unknown canopy variables. This has led to the use of semiempirical and empirical approaches. However, these models are usually site specific and therefore have a limited applicability outside of the conditions included in the data sets used in their development.

One approach to reducing the dimensionality of the problem is to characterize roughness and vegetation information using ancillary data sources. However, it is difficult to account for the spatial or temporal changes in these variables using ancillary data sources. Furthermore, errors in the ancillary sources could result in soil moisture estimation error.

An alternate approach to estimating the surface roughness and vegetation using the radar measurements themselves, in lieu of information from ancillary sources, is to use a time-series approach [8], [11]–[14]. In the time-series approach, both the vegetation and roughness [8], [11], [13] or only the roughness [14] is considered to remain stationary over a specific time window, during which soil moisture is assumed to be the only sources of variability in the signal. The challenge for the time-series approach is to identify measurements made within specific time windows inside which model components other than soil moisture could be considered constants.

Another approach to reducing the impact of surface roughness and vegetation in the retrieval of surface moisture status is to retrieve a soil moisture index that is relative between residual and saturation soil moisture levels. The residual and

Manuscript received May 29, 2014; revised October 21, 2014; accepted November 28, 2014.

P. S. Narvekar and D. Entekhabi are with the Department of Civil and Environmental Engineering, Massachusetts Institute of Technology, Cambridge, MA 02139 USA.

S.-B. Kim and E. G. Njoku are with the Jet Propulsion Laboratory, California Institute of Technology, Pasadena, CA 91109 USA.

Color versions of one or more of the figures in this paper are available online at http://ieeexplore.ieee.org.

Digital Object Identifier 10.1109/TGRS.2014.2377714

saturation soil moisture levels correspond to the minimum and maximum backscatter values, respectively [15]. These maximum and minimum backscatter values, however, may vary with time with changing vegetation and roughness conditions. The errors with finding the maximum and minimum backscatter values corresponding to the residual and saturation volumetric soil water content, respectively, add uncertainty. This approach also results in a relative soil saturation index and not volumetric soil moisture content.

Table I is a summary of these and other approaches developed for radar-based soil moisture and roughness estimation. These approaches, including those developed for frequencies other than the L-band, often allow soil moisture estimation only with the availability of ancillary data on roughness or other factors (reported as a column in Table I) [8], [10], [14], [16]–[25]. Zribi *et al.* [21] use the Z-parameter to parameterize roughness, Baghdadi *et al.* [22] suggest parameterization for correlation length, Paloscia *et al.* [20] introduced neural network and compares the performance with the other empirical methods, and Mattia *et al.* [18] and Lievens and Verhoest [24] modified roughness parameters to improve soil moisture estimates. Many of the algorithms use the integral equation model (IEM) and the Michigan Microwave Canopy Scattering (MIMICS) as building blocks or use outputs from these numerical models for algorithm training. Both these forward models require information on surface roughness and vegetation structure that is derived from ancillary information. The present approach is intended to investigate pathways for radar-based soil moisture retrieval that specifically does not require vegetation and roughness ancillary data. Furthermore, we seek an algorithm that could be considered for bare soils as well as vegetated areas in particular for testing new observations from the SMAP mission.

Several different algorithms are being considered for surface soil moisture estimation using SMAP radar measurements [8], [13], [15], [26]. Most of these methods use iterative algorithms to estimate soil moisture by minimizing differences between the computed and the observed backscatter (σ). Such approaches can be computationally challenging when applied to radar observations over continental scales with a 3-km spatial resolution. This problem can be overcome using a lookup table approach or "data cube" as demonstrated in [8], [14]. A data cube is a 3-D lookup table for σ computed using forward backscatter models for a wide range of the most significant three parameters: the roughness given as ks where $s = \mathrm{rms}$ (root mean square) height and $k = 2\pi/\text{wavelength}$, the vegetation water content (VWC), and the real part of the dielectric constant (ε). The lookup table for bare soils has only two dimensions, ks and ε [8]. The application of a lookup table in estimating soil moisture in snapshot and time-series mode is demonstrated in [14] for bare soil surfaces and [8] for vegetated surfaces. Data cubes have also been developed for a number of vegetated surface classes. The classes correspond to vegetation types, and for each, VWC is used as a proxy representation of all the vegetation properties for a given type of vegetation. Additional details on data cubes could be found in [8]. The accuracy of data-cube retrievals depends highly on how accurate the roughness and vegetation effects are accounted in ancillary data sources that determine ks and VWC.

In this paper, we use only radar observations at different polarizations to estimate vegetation and roughness effects. This is a research algorithm, and it is not intended to be part of the suite of science data products for the forthcoming SMAP mission.

The generalized formulation of the new algorithm is introduced in Section II. In Section III, this generalized formulation is evaluated at the limiting cases given by three end-members, defined as follows: 1) end-member I or smooth bare soils; 2) end-member II or rough bare soils; and 3) end-member III maximum vegetation surface. In order to make this approach independent of ancillary data requirements, we use the radar vegetation index (RVI) to account for vegetation effects [13] and scale between end-members. Initial studies of RVI show that it is related to microwave vegetation opacity (τ) [27], [28] and water content of the plant canopy. Roughness effects are incorporated using a new radar roughness index (RRI) introduced in Section IV that is also used to scale between end-members depending on the roughness conditions. In Section V, equations developed for limiting cases in terms of end-members are combined using RVI to obtain a generalized soil moisture estimation algorithm. In Section VI, the algorithm is tested using experimental observations. For this, ground-based POLARSCATTER bare soil data [29] and the Passive and Active L- and S-band (PALS) data obtained during the field campaigns of SGP99, SMEX02, CLASIC07, and SMAPVEX08 reported in [30] and SMAPVEX12 presented in [31] are used.

II. Basic Formulation

Backscatter observations over land principally depend on soil moisture, surface roughness, vegetation structure and the interaction between soil and vegetation. Modeling the scattering mechanisms comprehensively at a high spatial resolution over continental scales is computationally challenging [8], [29]. In this section, simple formulations are presented to represent approximate solutions for the complex electromagnetic scattering problem.

Based upon prior studies [2], [4], [29], a nonlinear formulation is necessary for bare soils in order to represent the backscatter dependence on surface volumetric soil moisture (m_v) [m^3 m^{-3}], whereas the linear formulation is found to adequately account for this dependence over vegetated areas [2], [11], [12]. Therefore, to account for the nonlinear and the linear dependence of σ on m_v in a single equation, we propose a generalized representation as

$$\sigma_{VV}[dB] = Sensitivity * m_v^{\lambda} + Intercept. \tag{1}$$

The vertical polarization is expected to have higher sensitivity to soil moisture than the horizontal polarization [2], [13], [29], and therefore, we have considered vertical polarization to represent backscatter (σ_{VV}) in terms of m_v in (1). *Sensitivity* and *Intercept* are functions of soil surface roughness and vegetation. They are discussed separately in Section II-A and B. The power term λ accounts for soil moisture dependence and is a function of vegetation level. For vegetated surfaces with a closed canopy, the $\lambda = 1$ linear formulation is used in [11], [12], and [32].

TABLE I
HERITAGE SURFACE SOIL MOISTURE RADAR RETRIEVAL ALGORITHMS

Reference Citation	Frequency & Polarizations	Parameters Retrieved	Ancillary Data Required	Surface Type	Algorithm Basis	Notes
Dubois et al. (1995) [6]	L-band; HH- & VV-Pol	m_v Roughness	Soil Texture	Bare Soil	Regression	Higher soil moisture sensitivity for VV-Pol reported
Shi et al. (1997) [7]	L- & C-band; HH- & VV-Pol	m_v Roughness	Soil Texture	Bare Soil	IEM	m_v estimated rmse ~ 0.04 [m^3m^{-3}]
Wagner et al. (1999) [15]	C-band; HH- & VV-Pol	Relative Soil Saturation Index	--	Bare Soil & Sparse Veg.	Change Detection	Tested Over Continental Scales
De Roo et al. (2001) [16]	L- & C-band; HH-, VV- & HV-Pol	m_v VWC	Crop Type	Sparse Veg.	MIMICS	Higher soil moisture sensitivity for VV-Pol reported
Bindlish and Barros (2001) [9]	C- & X-band; HH-, VV- & HV-Pol	m_v	Veg Type & Roughness	Sparse Veg.	Water-Cloud	
Zribi & Dechambre (2002) [17]	C-band; HH-Pol	m_v roughness	None	Bare Soil	Regression	Different Incidence Angles Used
Oh et al. (1992) [5]	L-band; HH-, VV- & HV-Pol	m_v roughness	None	Bare soil	Regression	Co-Pol Ratio Used for Roughness Estimation
Mattia et al. (2006) [18]	C-band; HH- & VV-Pol	m_v	*a priori* m_v & roughness	Bare Soil	Bayesian	A priori Information on m_v and Roughness
Joseph et al. (2008) [19]	L-band; HH- & VV-Pol	m_v roughness	Crop type	Veg. surfaces	IEM	Correction for Roughness and Veg. Effects
Palocia et al. (2008) [20]	C-band; HH- & HV-Pol	m_v	Veg./ Roughness	Bare Soil & Sparse Veg.	Neural Network	ANN Compared with IEM and Bayesian
Zribi et al. (2008) [21]	C-band /VV-Pol	m_v	NDVI	Bare Soil & Sparse Veg.	Regression	Tested over continental scale using ERS data from 1991-2000
Rahman et al. (2008) [42]	C-band / VV-Pol	m_v roughness		Bare Soil & Sparse veg.	Multi-Temporal	Tested over Southwest US
Kim & van Zyl (2009) [13]	L-band; VV- & HH - Pol	m_v	Roughness	Veg. surfaces	Change Detection	*RVI*
Pierdicca et al. (2010) [50]	C-band / VV-Pol	m_v	Optical Data	Sparse Veg.	Bayesian & IEM	Multi-Temporal
Baghdadi et al (2011) [22]	C-band/HV-Pol	roughness	m_v	Bare soil	Regression	Roughness Correlation Length
Balenzano, et al (2011) [23]	L- & C-band HH	m_v	Crop Type	Sparse Veg.	Regression	Co-pol Ratio Insensitive to Vegetation Change
Lievens & Verhoest (2011) [24]	L-band; HH-Pol	m_v	Crop type Roughness	Sparse Veg.	Water-Cloud	Roughness Adjusted to Improve m_v Estimates
Baghdadi et al (2012) [25]	X-band/ HH-Pol	m_v	Roughness	Bare Soil	Regression	Low Incidence Angle Has Higher Accuracy
Kim et al. (2012) [14]	L-band; HH- & VV-Pol	m_v Roughness	None	Bare Soil	Numerical Scattering Model	Different Bare Soil Models Compared
Kim et al. (2014) [8]	L-band; HH and VV-Pol	Roughness VWC m_v	VWC & Roughness	Bare Soil & Sparse Veg.	Numerical Scattering Model	Tested Over Global Scale and With Aquarius Data

Nonlinear (specifically $\lambda < 1$) dependence is used for bare soil and sparsely vegetated surfaces. The power term λ is discussed in Section II-C.

A. Sensitivity

Sensitivity to soil moisture, defined as the measure of change in σ with change in m_v, is denoted as $\Delta\sigma/\Delta m_v$ [32]. With linear formulations, it represents the slope of the regression line [13]. In this paper, we define the term *Sensitivity* to account for the soil moisture sensitivity at any given level of vegetation and roughness in the simplified form of (1).

Sensitivity is reported to be independent of roughness [7], but observations presented in Fig. 7 of [33], [35], and some recent studies, e.g., Fig. 5(b) of [34], show that the roughness also affects *Sensitivity* in addition to *Intercept*. In this paper, we incorporated the roughness dependence in both *Intercept* and *Sensitivity*.

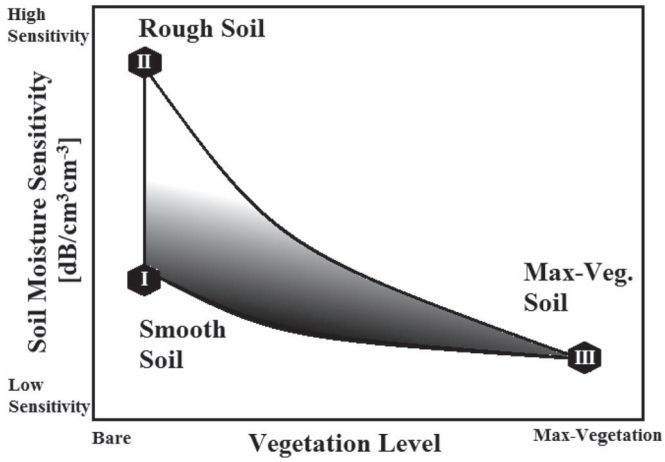

Fig. 1. Conceptual representation of *Sensitivity* in (1) with end-members enveloping possible sensitivities of backscatter to soil moisture. Sensitivity decreases with increasing vegetation (for nonforest moderate vegetation). Sensitivity increases with roughness for bare and sparsely vegetated surfaces.

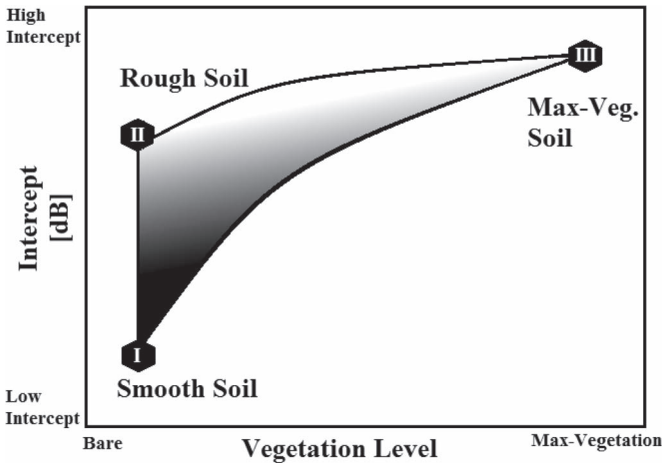

Fig. 2. Conceptual representation of *Intercept* in (1) with end-members enveloping possible sensitivities of backscatter to soil moisture.

Observations acquired over bare soils, such as data sets presented in Fig. 7 of [33], Fig. 5(b) of [34], and [35], show that the roughness increases *Sensitivity*. Moreover, in the presence of moderate vegetation, the *Sensitivity* could depend on surface roughness [32]. In this paper, to develop a general radar soil moisture algorithm at L-band, we have considered the increase in *Sensitivity* with roughness, and its formulation is discussed in Section III-B.

At off-nadir angles, with increasing amount of vegetation, *Sensitivity* monotonically decreases [3], [26]. For higher level of vegetation cover, the observed backscatter is primarily a function of vegetation cover (see [2, Ch. 21.5]). However, due to higher penetration of microwaves at L-band into the canopy, ground contribution is expected for vegetated surfaces with moderate vegetation, i.e., less than about 5-kg m^{-2} water content typical of agricultural fields, grasslands, and savannas [8].

In this paper, to address the *Sensitivity* in the form of (1), a conceptual diagram is introduced to represent *Sensitivity* variations from low to high vegetation and from smooth to rough bare soils [32]. The conceptual diagram is shown in Fig. 1. We define three end-members to envelop the maximum possible values that *Sensitivity* could take in (1). These end-members are defined as: 1) end-member I or smooth bare soil; 2) end-member II or rough bare soil; and 3) end-member III or maximum vegetation. The same end-members are also used to envelop possible *Intercept* values of (1).

B. Intercept

A conceptual representation of *Intercept* is shown in Fig. 2 [32]. *Intercept* is the backscatter value expected for dry soils. Over bare soils and under low vegetation condition, the *Intercept* defined in (1) is mainly a function of surface roughness, and as vegetation level increases, it becomes mainly a function of vegetation cover [2], [32]. Fig. 2 also depicts the same three end-members as those discussed for *Sensitivity* in Fig. 1. Moreover, based on [8] and [36], the *Intercept* could also depend on the type of vegetation based on the kind of scattering mechanism involved. In this paper, we do not account for these canopy structural effects. This will result in higher soil moisture retrieval errors, but it will be independent of errors in ancillary data on canopy structure. There are tradeoffs in error, and in this paper, we explore the approach of least reliance on ancillary information.

C. λ: Soil Moisture Functional Dependence

In (1), λ accounts for the relationship between σ and m_v and it is a function of vegetation. Observations show that rate of backscatter change due to changing m_v is higher when the soil moisture is approximately 0.2 m^3m^{-3} or lower and the rate is lower for soil moisture between this value and saturation [2]–[6]. To account for this trend, most of these bare soil surface models consider the nonlinear dependence of σ on m_v. Based on these models, λ could be shown approximately equal to 0.3. In this paper, we show that $\lambda = 0.3$ based on bare soil backscatter numerical simulations (see Section III-A). Over vegetated areas, the σ dependence on m_v is closer to linear [11]. Numerical simulations shown in Fig. 7(c) of [32] indicate a transition from nonlinear dependence (σ on m_v) in the case of bare soils to a linear dependence as the vegetation increases. Numerically, the power parameter λ of this dependence ranges from about 0.3 to 1.0, depending on the vegetation cover. In Section IV-A, we introduce the radar vegetation index (RVI) developed in [13] and [37]. The RVI is a normalized cross-polarization radar backscatter and approaches 1.0 for dense vegetation. It is bounded at zero for bare soils. The scale ranges of σ and RVI are similar and indicate the level of vegetation. We use RVI to account for the vegetation effect on λ, as will be shown in Section IV.

III. Evaluation of Three End-Members

Three end-members, i.e., end-member I or smooth bare soils, end-member II or rough bare soils, and end-member III or maximum vegetation cover, are defined to envelop the extremum expected values of *Sensitivity* and *Intercept* (see Figs. 1 and 2). Most surfaces are in between the end-members. In this section, we evaluate each of these end-members and establish quantitative values for them. We based our evaluations on numerical

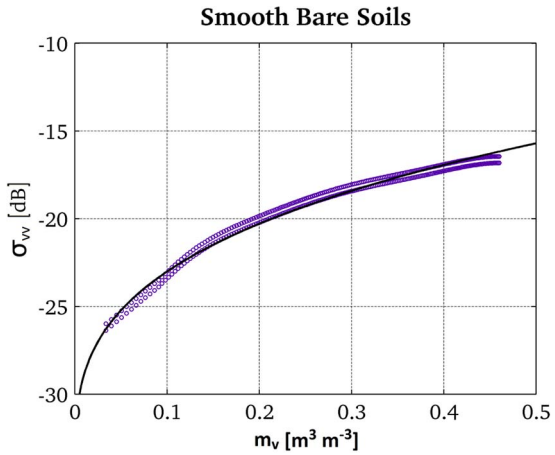

Fig. 3. Simulated σ_{VV} for bare soil data-cube values for $ks = 0.14$ to 0.16 (smooth bare soil surfaces) are plotted with the fit of (2). The fit represents end-member I. The data cube is based on numerical Maxwell solution in [29].

radar scattering model results available in the form of data cubes. The numerical simulations for bare soil surfaces with a range of roughness conditions are derived from [29]. These simulations solve the Maxwell equations in three dimensions and form reliable data for estimating the bare soil parameters for the retrieval algorithm. The dielectric constant model [38] is used where applicable to convert the dielectric constant to soil moisture. Furthermore, since SMAP observations will be made at a 40° incidence angle, the data-cube approach is available at a fixed incidence angle of 40° [8]. In this section, the possible values of *Sensitivity* and *Intercept* for three end-members are computed at 40° incidence using data cubes.

A. End-Member I: Smooth Bare Soils

Over smooth bare soils where roughness is not a primary influence, the observed backscatter could be considered to mainly depend on soil moisture. Therefore, based on (1), σ in terms of m_v for the smooth bare soil could be given as

$$\sigma^{ss}_{VV}[dB] = S_s * m_v^{\lambda} + \sigma^{\mathrm{s}}_{VV} \tag{2}$$

where σ^{s}_{VV} is defined as the minimum vertically polarized backscatter value expected for smooth bare soils and S_s is the *Sensitivity* of the backscatter to m_v. Both are functions of soil clay fraction clf. The dependence of S_s and σ^{s}_{VV} on soil texture is described in Appendix A. Over bare soils, smooth surfaces are defined using an upper limit of 0.6-cm rms height [8], [14]. Using the L-band wavelength k, the limit corresponds to $ks = 0.16$. For bare soil data cube, the lower roughness limit is considered as 0.14. Fig. 3 shows the backscatter simulated for ks values from 0.14 to 0.16, i.e., smooth conditions. Equation (1) fits the numerical Maxwell equation solutions [29] as shown in Fig. 3. This figure shows the case for soil texture with a clay fraction of 20%. This clay fraction is chosen since it is associated with loamy soil that comprises about 50% of the global soil category [30].

B. End-Member II: Rough Bare Soils

The soil surface roughness is usually defined in terms of rms height s and the correlation length l [4], [7]. Prior studies have shown that the IEM is suitable to account for a wide range of roughness conditions [4], [39]. The IEM could be modified using a general power law spectrum to relate s and l components [40], and therefore, the effect of s and l was shown to be comprehensively defined using a single term [41]. A similar study has also explored the relation between s and l using the IEM model [10], [42]. These studies noted a higher sensitivity of backscatter to s as compared to that of l. Recently, the impact of the correlation length is studied using the ratio l/s by Kim *et al.* [14] using the numerical solution for the bare surface scattering. In that study, the four values of $l/s(= 4, 7, 10,$ and $15)$ are considered (see [14, Fig. 8]). When dual co-polarized backscatter data are used for the retrieval, the impact of incorrect knowledge in l/s on the m_v retrieval is less than 0.015 $\mathrm{m^3 m^{-3}}$ [14]. In this paper, the roughness effect is considered using only s and ignoring the effect of l. This is a simplification and a potential source of error.

In order to account for the roughness effect in (1), the influence of roughness on both the *Sensitivity* and *Intercept* components must be considered (see Figs. 1 and 2). For bare soils, *Sensitivity* is usually considered almost independent of roughness, and the roughness effect is solely incorporated in the *Intercept* [14], [29], [39]. However, observations presented in Fig. 7 of [33], [35], and some latest studies, e.g., Fig. 5(b) of [34], show that the roughness also affects *Sensitivity* in addition to *Intercept*. In this paper, we incorporate the impact of roughness on *Intercept* as well as on *Sensitivity*. Therefore, for rough bare soil surfaces, we write (1) as

$$\sigma^{rs}_{VV}[dB] = S_r(ks) * m_v^{\lambda} + g(ks) \tag{3}$$

where S_r is the rough surface *Sensitivity* and g represents the rough surface *Intercept* both as a function of ks. We require that, as ks tends to 0, the $S_r(ks)$ and $g(ks)$ tend toward smooth soil parameters S_s and σ^{s}_{VV}, respectively, defined earlier in (2). Hence, we could write S_r in terms of smooth soil *Sensitivity* as

$$S_r(ks) = S_s * \{1 + f(ks)\} \tag{4}$$

where $f(ks)$ represents some function of ks that should tend to zero as ks tends to zero. Based on several approaches, such as [6], [26], [29], and [44], the logarithmic function with base 10 is shown to be a suitable function to adequately account for the dependence of σ on ks at a given m_v. In this paper, we used the $\log_{10}$ function to define $f(ks)$ in (4) as

$$S_r(ks) = S_s * \{1 + \log_{10}(1 + ks)\} \tag{5}$$

and the *Intercept* g as function ks can be simply written as

$$g(ks) = \sigma^{\mathrm{s}}_{VV} + \mathrm{C} * \log_{10}(1 + ks) \tag{6}$$

where the C parameter accounts for the roughness effect in dry soil condition, i.e., when m_v tends to zero. Substituting (5) and (6) in (3)

$$\sigma^{rs}_{VV}[dB] = S_s * \{1 + \log_{10}(1 + ks)\} * m_v^{\lambda} + \sigma^{s}_{VV} + \mathrm{C} * \log_{10}(1 + ks). \tag{7}$$

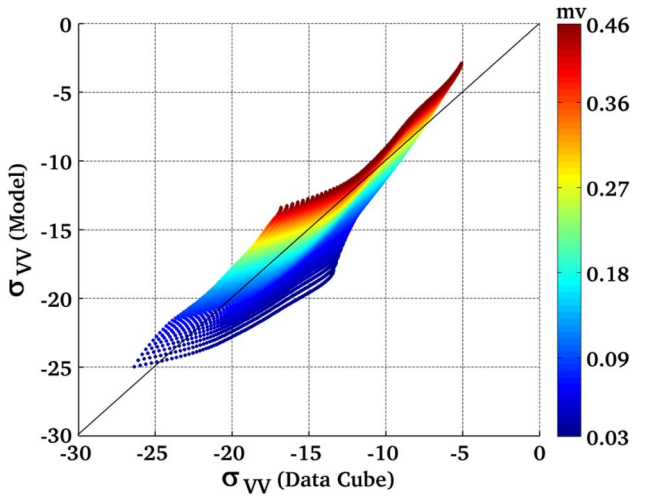

Fig. 4. σ_{VV} simulated for bare soils using (7) compared with numerical Maxwell solution [29] for all possible values of s from 0.5 to 4.5 cm.

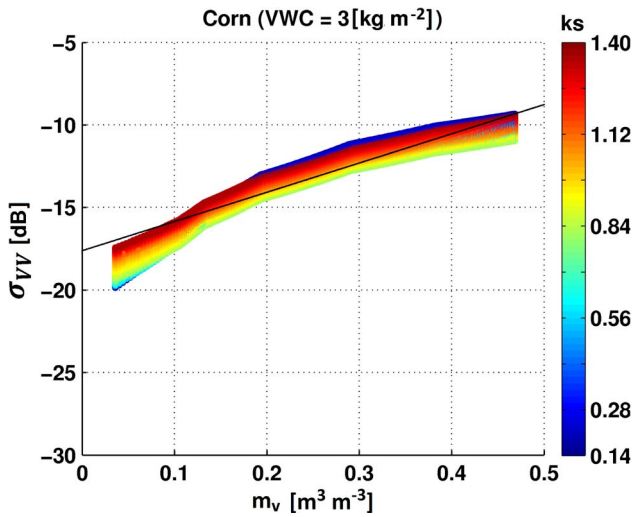

Fig. 5. σ_{VV} dependence on m_v for VWC $= 3$ kg m^{-2}. Under these conditions, the surface roughness has dampened effect on σ_{VV}.

Using bare soil data cube (derived from the numerical solutions to Maxwell equations [29]) for ks ranging from 0.14 (smooth) to 1.4 (rough) (the range considered in bare soil data cube) [14], C is estimated as $C = 13.6$.

For example, for soil texture corresponding to a typical clay fraction of 20%, Sr defined in (5) ranges from 23.00 to 31.75, and g given in (6) ranges from -34.50 to -29.33 for ks varying from 0.14 to 1.4 (corresponding to s from 0.5 cm to 4.5 cm). These ranges of modulation in *Sensitivity* and *Intercept* could be used to account for the sensitivity dependence on roughness for low vegetation [32] and some bare soil observations presented in [33]. In this paper, end-members I and II are associated with bare soils, and therefore, we evaluate (7) using the theoretical model available to us in the form of the numerical solution of Maxwell equations [29], as shown in Fig. 4. In this figure, the σ_{VV} values estimated using (7) are compared with those obtained from the bare soil data cube based on [29]. The new formulation fits the data cubes within the accuracy of $\mathrm{rmse(root\ mean\ square\ error)} = 1.2$ dB and a correlation of 0.97. It should be noted that Fig. 4 does not present statistical samples, so the correlation and rmse are just the indicators of agreement between newly developed formulations and the numerical scattering solution available to us in the form of bare soil data cube.

C. End-Member III: Maximum Vegetation

Recently, significant efforts have been made to model the backscatter observed over different types of vegetation using electromagnetic scattering theory [8], [36]. The range of the backscatter variation over vegetated areas depends on both the type or architecture of vegetation and VWC level [8]. In this paper, the relationship between σ and m_v under maximum possible vegetation condition follows (1):

$$\sigma_{VV}[dB] = \gamma * m_v^{\lambda} + \sigma_{VV}^{\mathrm{vf}} \tag{8}$$

for end-member III. Here, γ and $\sigma_{VV}^{\mathrm{vf}}$ are *Sensitivity* and the *Intercept* of the maximum vegetation scattering conditions. Maximum vegetation is defined as a canopy cover that dominates the radar backscatter and reduces sensitivity to soil moisture, hence the convergence to a point (end-member III in Figs. 1 and 2). This level is generally considered to be moderate woody vegetation (closed canopy bushes and trees) and mature crops. The vegetation water content under these conditions is 3 to 5 kg m^{-2}. The conditions of strong double-bounce scattering were excluded in this study because, there, the soil moisture is still a dominant factor. The magnitude of m_v contribution in the observed backscatter under vegetated condition depends on scattering among soil and vegetation components. The values of γ and $\sigma_{VV}^{\mathrm{vf}}$ depend on the type of vegetation [8], [36]. The parameters of (8) for different vegetation types are estimated using vegetation data cubes reported in [8]. The vegetation data cubes include 12 individual vegetation classes that are based on the International Geosphere-Biosphere Program (IGBP) classification schemes. The additional cropland classification database was incorporated to further specify the IGBP crop layer into four major crops: wheat, corn, rice, and soybean [8]. As discussed earlier based on Figs. 1 and 2, the soil surface contribution decreases with increasing vegetation level (again except for the double-bounce regimes that are beyond the scope of this paper). At around VWC $= 3$ kg m^{-2}, the modulation

TABLE II
EQUATION (8) PARAMETERS AT VWC $= 5$ kg m^{-2} REPRESENTING MAXIMUM VEGETATION CONDITIONS

Data Cube	Parameters for Eq. (9) obtained at VWC = 5 [kg m^{-2}]		Eq. (9) compared with data cubes simulations for all VWC>=5 [kg m^{-2}]		
	γ	$\sigma_{VV}^{\mathrm{vf}}$	rmse (dB)	bias (dB)	corr.
Grass	8.96	-17.34	1.41	0.00	0.60
Open/Closed Shrubs	19.17	-7.84	2.72	0.00	0.63
Crop/Nat	16.89	-12.18	2.07	0.00	0.69
Corn	18.41	-19.10	1.46	0.00	0.83
Deci.Broad	13.20	-12.33	0.91	+0.30	0.88
Deci.Needle	6.69	-12.44	1.27	+1.00	0.58
EverGrnBroad	9.47	-13.99	2.34	+1.98	0.43
EverGrnNeedle	14.75	-7.73	3.18	-0.23	0.52
MixedForest	13.30	-9.81	2.14	+0.44	0.61

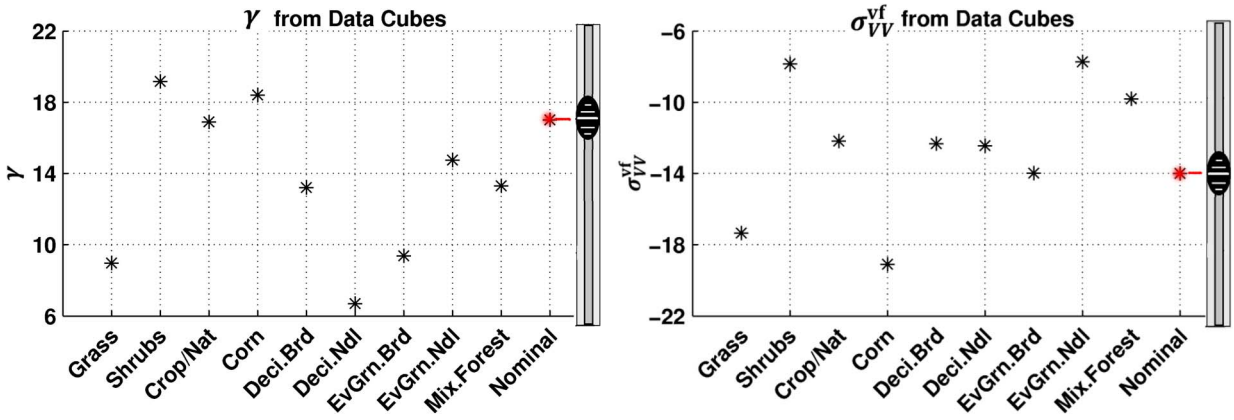

Fig. 6. Vegetated end-member III *Sensitivity* and *Intercept* parameters for different surface types. Nominal vegetation parameters selected are $\gamma = 17$ and $\sigma_{VV}^{\mathrm{vf}} = -14.0$.

in the observed backscatter due to varying roughness could be considerably lower than that due to varying m_v; an example of corn is shown in Fig. 5. The linear formulation of (8) fits well at this level with $\mathrm{rmse} = 0.74$ dB and a correlation of 0.94. It should be noted that Fig. 5 does not present statistical samples, so the correlation and rmse are just the indicator of agreement between linear approximation and data cube simulation at VWC $= 3$ kg m^{-2}. Above this VWC, as vegetation level approached the expected maximum level, i.e., VWC $=$ 5 kg m^{-2}, the backscatter may slightly decrease with increasing roughness [8], causing slightly higher scatter around the linear fit, resulting in $\mathrm{rmse} = 1.46$ dB and a correlation of 0.83. For most of the nonwoody vegetation, the maximum VWC level is considered to be 5 kg m^{-2} (see [8, Table I]). Therefore, to obtain the parameterization of (8) for all available data cubes, we set VWC $= 5$ kg m^{-2}. Table II lists the parameters of (8) at VWC $= 5$ kg m^{-2}. Additionally, as reported in [8], for woody vegetation, VWC may be well above 5 kg m^{-2}. Therefore, Table II also presents validation (8) with data cube simulations for VWC > 5 kg m^{-2}. For grass, Sensitivity is low. The grass canopy may act as an attenuation layer minimizing sensitivity to soil surface, whereas for croplands or shrubs, sensitivity is comparatively high due to higher order scattering between soil and vegetation components [8]. Some errors are expected because (8) assumes insensitivity at ∼5 kg m^{-2} VWC, but data cubes include the double-bounce processes that are dominant at 5 kg m^{-2} (for corn).

In order to minimize the reliance on uncertain land classification ancillary data and minimize the dependence on the vegetation data cubes, we select nominal parameters for end-member III [see (8)]. The nominal parameters are applied globally in order to allow radar-only retrievals without ancillary land-use and canopy structure information. The level of vegetation is still accounted for in the retrieval algorithm (see Section IV-A). Fig. 6 shows the vegetation data cube estimates for γ and $\sigma_{VV}^{\mathrm{vf}}$. Also, shown are the nominal global parameters.

IV. Vegetation Level and Roughness Level Indices

In this section, vegetation and roughness effects on *Sensitivity* and *Intercept* within the regions bounded by the three end-members (see Figs. 1 and 2) are addressed. Even though the roughness and vegetation parameters for a particular land surface may be known based on ancillary data, it is usually difficult to accurately account for and monitor changes in these variables over time. Ideally, roughness and vegetation information derived from the same radar instrument should be used. In this paper, we use RVI for vegetation and introduce a new (RRI). These two radar-derived indices are used to modulate the *Sensitivity* and *Intercept* parameters for conditions in between the three end-members.

A. RVI

The RVI defined in [13] characterizes the vegetation volume scattering as a normalized index as

$$RVI = \frac{8 \cdot \sigma_{HV}}{\sigma_{HH} + \sigma_{VV} + 2 \cdot \sigma_{HV}}. \tag{9}$$

The RVI is expected to be indicative of the magnitude of scattering by vegetation, and its value saturates at the unity when radar return power is dominated by vegetation volume scattering. When the volume scattering by vegetation dominates, $\sigma_{HH} = \sigma_{VV} = 3 \cdot \sigma_{HV}$ [13], [37], resulting in $RVI = 1$. A previous study [27] has shown a correlation of up to 0.9 between RVI and vegetation microwave optical depth τ. Moreover, a study in [28] compared the RVI at X-, C-, and L-bands for the rice and the soybean canopy. That study also demonstrates that the L-band RVI has the potential to account for the vegetation dielectric effect. In this paper, RVI is used to quantify and account for the level of the vegetation scattering.

B. RRI

It is difficult to accurately account for the surface roughness effects over a sensor footprint and to separate soil surface roughness effects from vegetation roughness effects in the backscatter. Ancillary information on roughness at the global scale and on roughness temporal variability is indirect and unreliable. Therefore, information derived from the same sensor, such as RVI discussed for vegetation, could be a more reliable source. Earlier studies have shown the sensitivity of copolarized backscatter ratio to s [5], [10], [44]. Here, we define

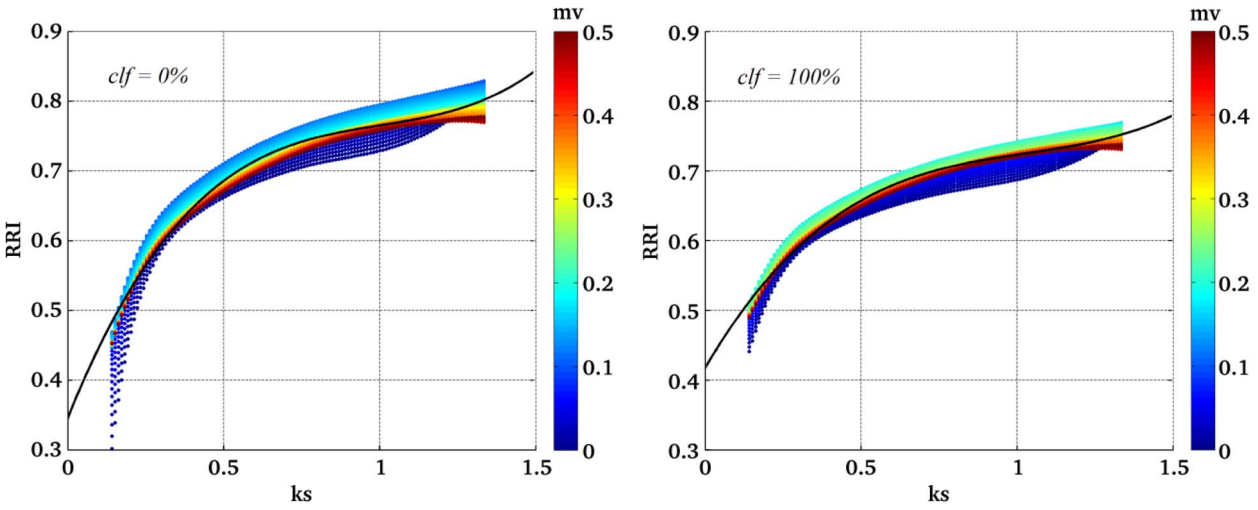

Fig. 7. RRI simulated from bare soil data cube at clf of 0% and 100% versus ks. The color scale represents the m_v value in $\mathrm{m^3m^{-3}}$. The lines represent the third-degree polynomial fit.

a new modified ratio considering parameters associated with end-member I (smooth bare soils)

$$RRI = \frac{\sigma_{HH} - \sigma^s_{HH}}{\sigma_{VV} - \sigma^s_{VV}} \tag{10}$$

where σ_{VV} and σ_{HH} represent observations and σ^{s}_{VV} and σ^{s}_{HH} are the constant minimum bare soil backscatter values. σ^{s}_{VV} and σ^{s}_{HH} are estimated based on the electromagnetic approach shown earlier for (2) and are provided as a function of soil texture in Appendix A. Fig. 7 shows the RRI plotted with ks for two different soil textures corresponding to extreme levels of clay fraction of 0% and 100%. There appears to be a systematic relationship between the simulated RRI and ks. The third-degree polynomial function is used to characterize the relationship between the RRI given in (10) and ks as shown with the line fit in Fig. 7. Since there is no significant effect of clay fraction on RRI, we consider a polynomial fit at $clf = 0.2$, given as

$$RRI = 0.3034ks^3 - 0.9203ks^2 + 0.9989ks + 0.3910. \tag{11}$$

This clay fraction is the most common (modal) soil classification [30] across global nonfrozen land regions. The accuracy of these estimates based on RRI is tested using ground-based POLARSCATTER bare soil observations discussed hereinafter in Section VI.

V. Generalized Radar Algorithm

A weighting approach is used to merge the bare soil and vegetation formulations developed in Section III based on RVI as

$$\sigma_{VV}[dB] = RVI * \sigma^v_{VV} + (1 - RVI) * \sigma^{rs}_{VV}. \tag{12}$$

Substituting for $\sigma^{\mathrm{rs}}_{VV}$ and σ^v_{VV} from (7) and (8) and rearranging in the form of (1) result in

$$\begin{aligned}\sigma_{VV}[dB] = {} & (RVI * \gamma + (1-RVI) * \{1 + \log_{10}(1+ks)\} * S_s) \\ & * m_v^{\lambda} + (1 - RVI) * (\sigma^s_{VV} + \mathrm{C} * (\log_{10}(1 + ks)) \\ & + RVI * \sigma^{\mathrm{vf}}_{VV}.\end{aligned} \tag{13}$$

The retrieval model parameters are S_s, σ^{s}_{VV}, γ, σ^{vf}_{VV}, and C. They are associated with the end-members and described in Section III and in Appendix A. As discussed earlier in Section II-C, based on the simulations presented in Fig. 7(c) of [32], the power term λ (indicator of vegetation level) takes values in the range of 0.3–1.0 to account for vegetation level from thin to dense. This range is also associated with RVI, which is also an indicator of vegetation level as reported in [13] and [28]. Therefore, λ in terms of RVI is simply given as

$$\lambda = RVI, \text{ for } RVI > 0.3 \text{ and } \lambda = 0.3, \text{ for } RVI <= 0.3. \tag{14}$$

Based on (13), the backscatter nonlinearly depends on m_v for bare soils, and as the vegetation level increases, this equation approaches linear formulation. This approach is compatible with the earlier study reported in [32].

The ks in (13) is estimated using RRI which is formulated for bare soils. Its application to moderate vegetation conditions is likely to reduce algorithm performance (shown in the following section). However, as the vegetation level increases, the bare soil contribution in (13) decreases. Therefore, the observed level of rmse in ks estimates under vegetation condition could affect m_v and they are estimated to be $\mathrm{rmse} < 0.01$ $\mathrm{m^3m^{-3}}$. The performance of the algorithm using different field campaign observations is discussed in the next section.

VI. Evaluation Using Field Campaign Observations

To demonstrate the performance of the algorithm, the L-band radar observations acquired during several field campaigns and covering a wide range of vegetation and roughness conditions are used. These include the bare soil ground-based observations acquired in Michigan and airborne observations acquired from the series of heritage L-band PALS experiments from 1999 to 2008 reported in [30] and more recent PALS data acquired during SMAPVEX12 [31]. The quality of estimated m_v is tested against *in situ* observed m_v using rmse, bias, and bias-removed rmse. The bias-removed rmse or unbiased rmse (ub_rmse) [46]

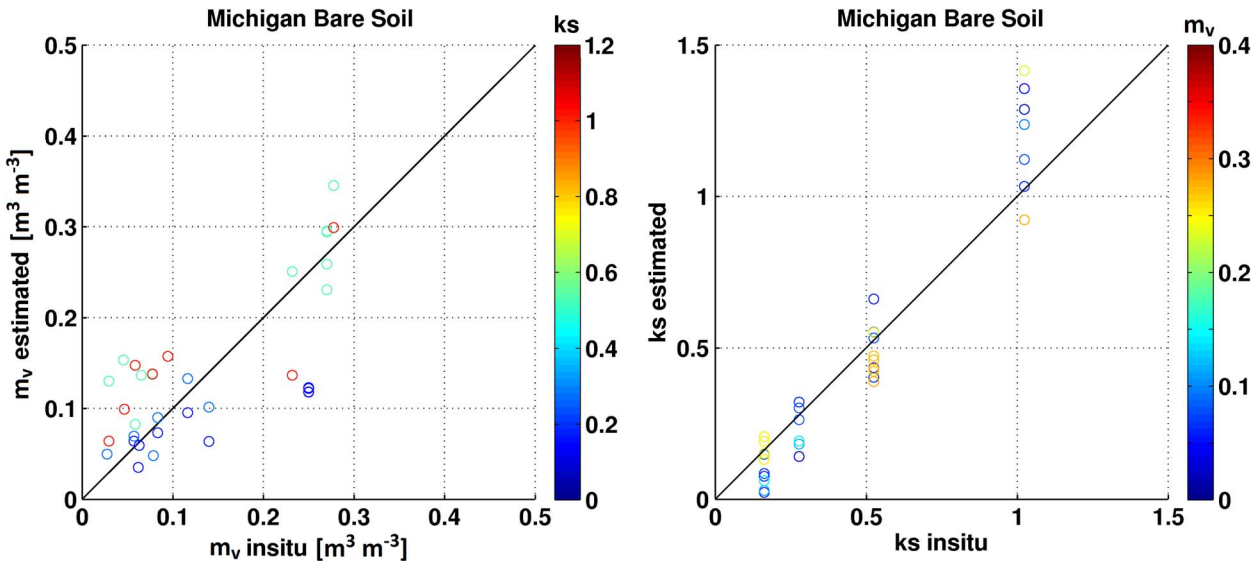

Fig. 8. Algorithm tests using Michigan bare soil field measurements for m_v and ks. Table III lists the statistics of the comparison.

TABLE III
RESULTS FOR GROUND-BASED BARE SOIL OBSERVATIONS FROM MICHIGAN

Maxwell equations numerical solution-based parameters								
$S0$	σ^{s0}_{VV}	σ^{s0}_{HH}	m_v estimates			ks estimates		
			ub_rmse [m^3m^{-3}]	bias [m^3m^{-3}]	corr.	ub_rmse	bias	corr.
20.6	-32.3	-29.3	0.070	+0.020	0.74	0.169	+0.050	0.97
Optimized parameters								
$S0$	σ^{s0}_{VV}	σ^{s0}_{HH}	m_v estimates			ks estimates		
			rmse [m^3m^{-3}]	bias [m^3m^{-3}]	corr.	rmse	bias	corr.
24.6	-33.7	-30.0	0.065	0.00	0.72	0.132	0.00	0.97

accounts for the random error in the data, and it is equivalent to isolating the standard deviation in the error when the bias is removed. We report both unbiased rmse and bias, which are constituting elements of the total rmse but indicate different types of error.

A. Michigan Ground-Based Observations

Bare soil observations made with a truck-mounted instrument called POLARSCATTER are used to test the treatment of bare soil conditions in the retrieval algorithm. These observations were made in agricultural fields near Ypsilanti, Michigan, and rereported in [29]. The comparisons of the field observations and the proposed algorithm for bare soils are shown in Fig. 8. The results are compared for data cube-based parameters and optimized parameters (see Table III). The soil moisture rmse by using optimized parameters is 0.065 m^3 m^{-3} with a correlation of 0.72. The *Sensitivity* $S0$ is higher than our *a priori* value. Such differences in sensitivities were also observed in earlier studies [13]. These differences are also observed when using PALS observations, and they are discussed later. A unique feature of the retrieval algorithm introduced here is that the estimation is snapshot with no ancillary roughness information required. The ks estimation is a part of the retrieval process, which is used for m_v estimation. There were only 34 points, most of which were on the 1:1 line for all roughness levels (see Fig. 8). The quality of ks estimates using (11) is also shown in Fig. 8. A low $\mathrm{rmse} = 0.13$ and a correlation of 0.95 show the reliability of using RRI for accounting the roughness effect.

B. PALS Airborne Field Experiments

The PALS instrument is an airborne sensor flown during various field campaigns since 1999. In this paper, we use PALS data and *in situ* soil moisture observations acquired during SGP99, SMEX02, CLASIC07, and SMEPVEX08 reported in [30] and SMAPVEX12 reported in [31]. The PALS had flown on board different aircrafts and had different antenna setups during different field campaigns [27], [30]. Therefore, data acquisition methods differ from campaign to campaign, but the operational characteristics, such as frequencies, polarizations, and the look angle ($\sim 40^\circ$), are the same for all campaigns [27], [30].

During SGP99, the PALS data were acquired over a study area of 7 $\times$ 41 km across the Little Washita watershed in Oklahoma in 1999 [11]. The experiment area is dominated by grass cover [30]. Again, during CLASIC07, data were

TABLE IV
RESULTS FOR PALS AIRBORNE OBSERVATIONS FROM DIFFERENT FIELD CAMPAIGNS

Nominal Parameters

Field exp. (# of obs.)	$S0$	σ^{s0}_{VV}	σ^{s0}_{HH}	γ	σ^{vf}_{VV}	ub_rmse [m^3m^{-3}]	bias [m^3m^{-3}]	corr.
SGP99 (78)	20.6	-32.3	-29.3	17.0	-14.0	0.059	-0.052	0.63
SMEX02 (208)						0.072	-0.010	0.59
CLASIC07 (294)						0.110	-0.070	Not Signif.
SMAPVEX08 (199)						0.067	-0.008	Not Signif.
SMAPVEX12 (433)						0.084	+0.003	0.51

Optimized Parameters

Field exp. (# of obs.)	$S0$	σ^{s0}_{VV}	σ^{s0}_{HH}	γ	σ^{vf}_{VV}	rmse [m^3m^{-3}]	bias [m^3m^{-3}]	corr.
SGP99 (78)	25.5	-36.5	-31.9	20.0	-15.8	0.055	0.00	0.66
SMEX02 (208)	25.0	-35.7	-34.0	19.7	-18.0	0.067	0.00	0.55
CLASIC07 (294)	28.2	-35.4	-28.0	18.2	-17.6	0.097	0.00	Not Signif.
SMAPVEX08 (199)	24.4	-36.5	-31.6	20.0	-13.4	0.057	0.00	Not Signif.
SMAPVEX12 (433)	20.9	-37.5	-29.1	16.8	-7.4	0.067	0.00	0.72

acquired over study areas of 6×52 km across Little Washita and 3×28 km at Fort Cobb in Oklahoma in 2007 [47]. During CLASIC07, the area under observation includes cropland, with the winter wheat as the dominating crop [30]. During SMEX02, data were acquired at the Walnut Creek watershed in Iowa in 2002, primarily an agricultural region with corn and soybean being the dominant crops [12]. The SMAPVEX08 was carried out at Choptank in Maryland in 2008, which is a mixed agriculture field with corn (senescence stage), soybean, and forest [30]. The SMAPVEX12 field experiment was carried out in Canada. The experiment domain mainly included diverse agricultural fields [31]. During that experiment, at least ten surface types were observed by the PALS, including soybean, corn, wheat, winter wheat, oat, canola, corn/granola, beans, forage, and pasture. The topography for all the areas was not significantly variable. The primary soil texture of all the fields, except SMAPVEX12, falls under the loamy soil category, and the clay fraction for all the fields is mostly below 25% [30]. The land surface conditions observed during SMAPVEX12 were more diverse in terms of soil texture and VWC level when compared to other PALS experiments.

The soil texture over the SMAPVEX12 domain can reach a 70% clay fraction, and the vegetation cover for most of the crop fields had higher levels of VWC, exceeding 3 kg m^{-2}. During the PALS field campaigns, wide dynamic ranges of *in situ* soil moisture are observed, except for CLASIC07 and SMAPVEX08. For those two experiments, most of the *in situ* soil moisture values were moist (above 0.2 m^3 m^{-3}) with little dynamic range.

PALS observations for SGP99 and SMEX02 were resampled at ∼0.4 km, and for CLASIC07 and SMAPVEX08, observations were resampled at ∼0.6 km and ∼1.8 km, respectively [30]. The SMAPVEX12 data were not available for [30]. For this paper, PALS data acquired during SMAPVEX12 and resampled at a 1.6-km grid matching with *in situ* soil moisture observations are used.

C. Calibration Bias in PALS

We detect biases between the backscatter observations acquired from the feed-horn antenna (during SGP99 and SMEX02) and from the patch array antenna (during SMEX02 and SMAPVEX08). Unlike radiometer observations, radar observations could not be calibrated using vicarious targets like water bodies. The field of view of the instrument covers a large region, and corner reflectors cannot be used for radar calibration. In this paper, biases associated with radar PALS observations are estimated based on differences observed between ranges of backscatter data over the same land cover type during different field campaigns and in reference with T_B observations. The difference between the ranges of backscatter observed from the feed horn and patch array are studied with grass pixels for SGP99 and CLASIC07 and with corn pixels for SMEX02 and SMPAVEX08. These experiment domains consist of similar soil texture and mostly loamy soil [30]. Differences observed between the mean values of two distributions are $\Delta\sigma_{HH} = 3.23$ dB, $\Delta\sigma_{VV} = 4.50$ dB, and $\Delta\sigma_{HV} = 4.66$ dB, where $\Delta\sigma = \text{patch} - \text{horn}$. Therefore, we considered a bias correction of $+4.5$ dB in σ_{VV}, $+3.23$ dB in σ_{HH}, and $+4.66$ dB in σ_{HV} for SGP99 and SMEX02 observations.

D. Results With PALS Observations

A newly developed algorithm is applied separately for each field campaign. Table IV summarizes the results obtained for PALS field campaigns with nominal model parameters and

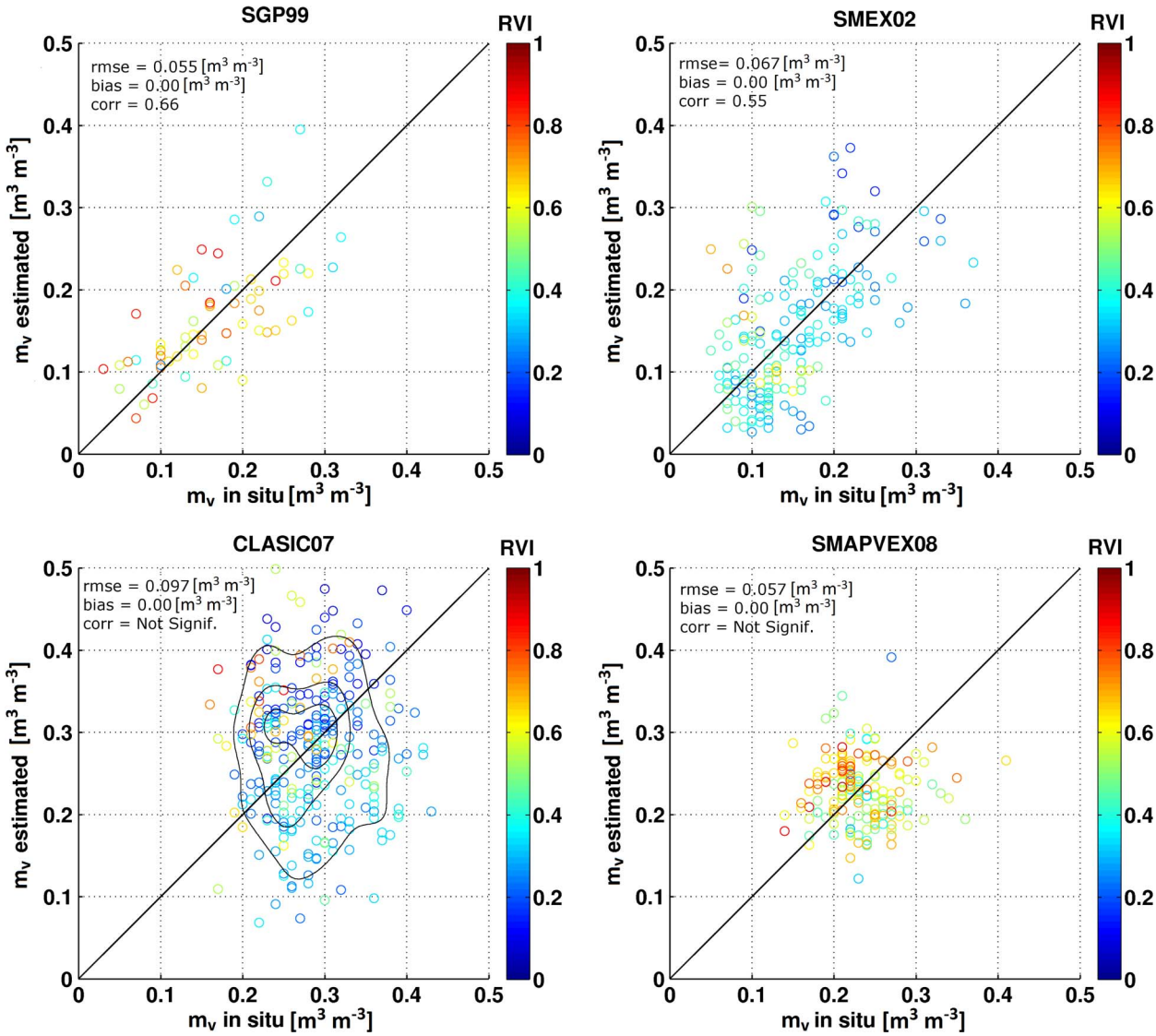

Fig. 9. Retrieved soil moisture compared with *in situ* soil moisture for SGP99, SMEX02, and CLASIC07 at Little Washita and Fort Cobb and SMAPVEX08 using optimized parameters. The statistics reported in Table IV include both nominal and optimized parameters.

optimized model parameters. The nominal parameters are reported in Fig. 8. Optimized parameters are estimated for each field campaign. The comparison of the two is an indicator of the maximum error expected by fixing the retrieval model parameter values for global application. Although the field experiment domains do not cover the diversity of global vegetation, the comparison should be an indicator of the expected error.

Figs. 9 and 10 show the scatterplots comparing estimated and *in situ* m_v. Optimized parameters result in large improvements in rmse for the SMAPVEX12 cases and large improvements in bias for the SGP99 and CLASIC07 cases. For the bare soil component of the algorithm, the optimized *Sensitivity* $S0$ is higher, and the *Intercept* σ^{s0}_{VV} is lower for the optimized parameters when compared to the nominal (see Table IV). The exception is SMAPVEX12. Similar differences between the observed and the nominal sensitivity of backscatter to soil moisture are discussed in [13]. The radar responses, particularly at lower frequencies such as L-band, are impacted by subsurface effects [48]. Under some conditions, the observed backscatter may be lower than the theoretically predicted backscatter [49]. The bare soil data cube used to estimate model parameters for this paper does not incorporate subsurface effects. Furthermore, the lower roughness limit for estimating the bare soil component is $ks = 0.14$, the smallest value used in the bare soil data cube. For SMAPVEX12, the ks values lower than 0.14 were observed as apparent in Fig. 10. This may be an additional reason for the lower value of optimized σ^{s0}_{VV} for this experiment.

The differences between optimized and nominal vegetation parameters are small for the field experiments except for SMAPVEX12 (see Table IV). The intercept value is in the range for shrubs or mixed forest (vegetation types discussed in [8]) and shown in Fig. 6. These vegetation types are expected to have higher levels of VWC, and therefore, the backscatter observed may be higher when compared to vegetation with low VWC. SMAPVEX12 contained crop fields with high VWC which contribute to a higher *Intercept*.

For CLASIC07, the $\mathrm{rmse} = 0.097$ $\mathrm{m^3 m^{-3}}$ observed is considerably higher compared to other experiments (see Fig. 9).

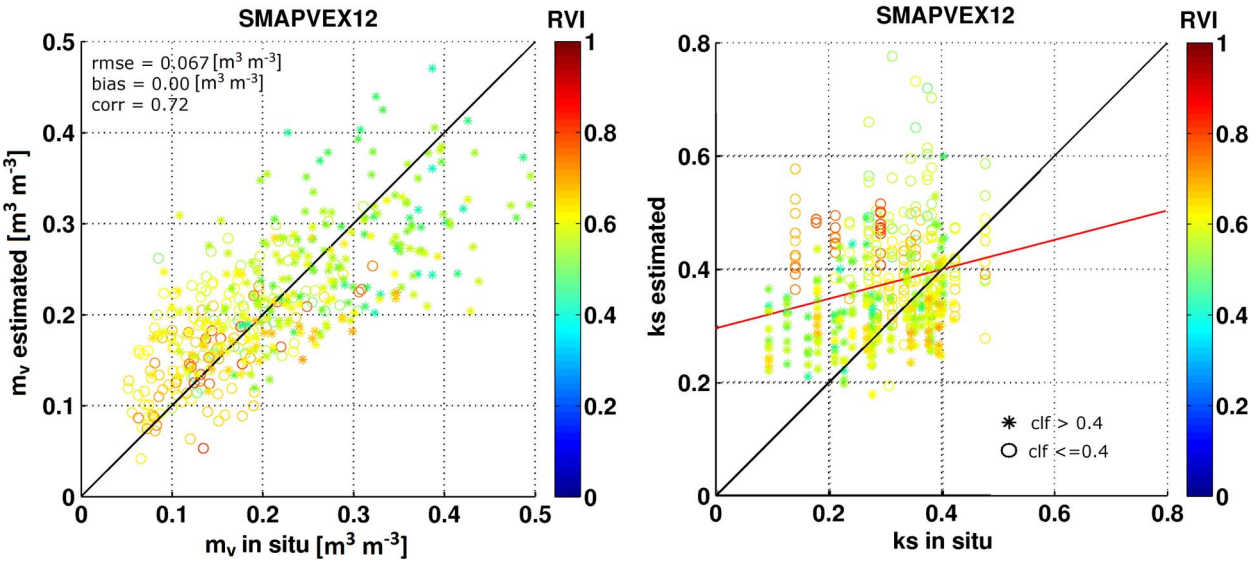

Fig. 10. Retrieved soil moisture is compared with *in situ* soil moisture for SMAPVEX12. The rmse and bias statistics are reported in Table IV. The different marker types distinguish different levels of clay fraction.

This is comparable with the average rmse observed for CLASIC07 in a previous algorithm study with PALS radar observations ($\sim$0.1 $\mathrm{m^3m^{-3}}$ [47]). The higher rmses observed are related to experimental conditions. During CLASIC07, there was standing water in some of the fields. Higher scatter for such crop fields may be expected since vegetation in standing water may act as a strong reflector. The contours in Fig. 9 each enclose about 90 data pairs. They generally encompass the 1:1. For SMAPVEX08, the observed dynamic range of soil moisture was smaller. The $\mathrm{rmse} = 0.057$ $\mathrm{m^3m^{-3}}$ results from the comparisons of the retrieval and the ground truth. The results for SMAPVEX08 are based on 199 data pairs. The agreement is an indicator of the potential of the radar-only model to estimate m_v under diverse land surface conditions.

The results shown for SMAPVEX12 in Fig. 10 and Table IV are for the highest number of ground truth matched data points (numbering 433) compared to other field experiments. The ub_rmse with nominal parameters is larger than those obtained for the earlier field experiments. The land surface conditions during SMAPVEX12 were diverse in terms of soil texture, range of crop types, and VWC levels, when compared to earlier PALS experiments. The soil texture observed for the SMAPVEX12 domain consists of clay percentage ranging on the order of 4% to 70%. Therefore, uncertainties in accounting correctly for the soil texture condition over a 1.6 $\times$ 1.6 km area may be one reason. To study the effect of clay fraction on retrieval, two levels are shown in Fig. 10, $clf <= 0.4$ and $clf > 0.4$ considering optimized parameters. The rmse for m_v estimates is 0.051 $\mathrm{m^3m^{-3}}$ for $clf < 0.4$. However, for higher levels of clf (i.e., $clf > 0.4$), the rmse increases to 0.073 $\mathrm{m^3m^{-3}}$. The unusually high clay content may be a contributing factor to the error.

Finally, the potential of RRI in accounting for ks effect also under vegetated conditions is demonstrated in Fig. 10. The *in situ* ks observations vary between 0.1 and 0.5, and the estimated ks varies between 0.2 and 0.6. The estimated rmse is 0.14 which includes a bias of +0.07. A regression line is added to the plot to show the relation between the measured estimated ks and *in situ* observations. Mainly, points with $clf <= 0.4$ show some overestimation compared to *in situ*; otherwise, there is a considerable agreement between the ks estimates and *in situ*.

VII. Summary

A new algorithm for surface soil moisture mapping using L-band radar observations is developed that is designed not to require ancillary information on surface roughness and vegetation. A simple formulation based on heritage and established relationships is used to represent backscatter dependence on soil moisture for limiting cases defined by three end-members: 1) end-member I or smooth bare soils; 2) end-member II or rough soils; and 3) end-member III or maximum vegetation cover. These end-members are used to envelop backscatter expected for intermediate land use and land cover. In order to make the approach independent of ancillary data, we use the (RVI) formed from radar measurements alone to account for the variable vegetation effect. We introduce a new (RRI) also formed from radar observations alone to account for variable roughness effects. The RVI and RRI scale the model parameters between the end-members. They only depend on radar backscatter observations and do not require ancillary data on vegetation and roughness. Clay fraction has a large effect, and its effects are taken into account (Appendix A). Using this algorithm, the m_v can be estimated in a computationally efficient manner for generating a near real-time soil moisture product.

The observational data sets used for testing the algorithm included the bare soil ground-based observations acquired from truck-mounted radar and airborne observations acquired by PALS during SGP99, SMEX02, CLASIC07, SMAPVEX08, and SMAPVEX12. The nondimensional surface roughness ks

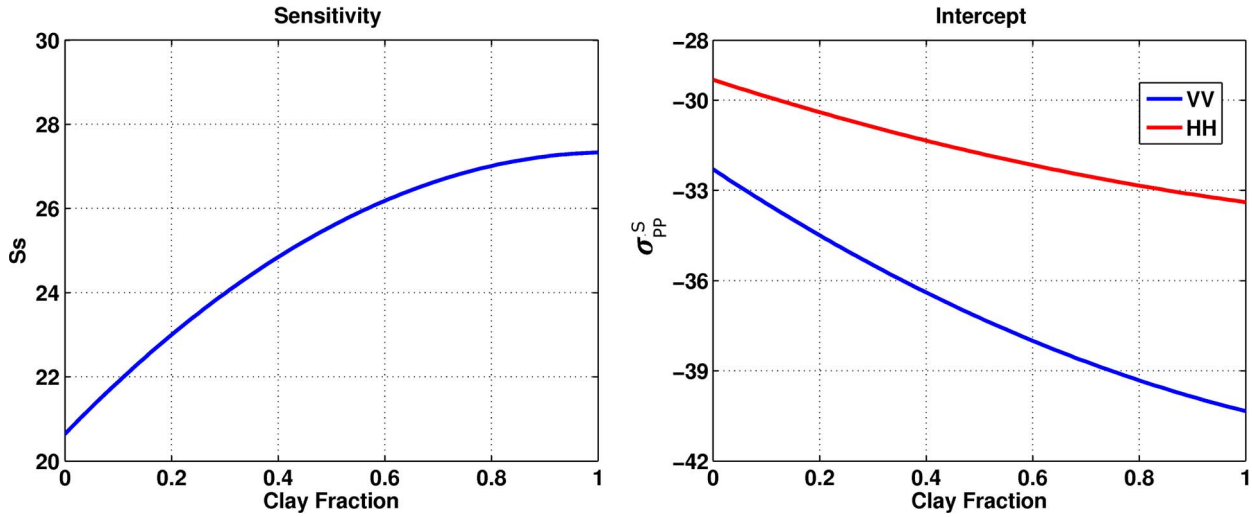

Fig. 11. *Sensitivity* (S_s) and *Intercept* (σ^s_{PP}) (VV and HH) values computed for different clay fraction.

metric using RRI shows agreement for bare soils and a clear sensitivity for *in situ* ks also under dense vegetation conditions. For SGP99, SMAPVEX08, and SMAPVEX12 (for clay fraction $<= 0.4$), the rmses were below 0.06 m^3 m^{-3}, which is within the quality target set for the SMAP radar-only m_v product. The SMAPVEX12 data allowed the testing of the newly developed algorithm for a wide variety of croplands with a high level of VWC. Due to very diverse land surface conditions observed for SMAPVEX12, results observed for this domain are expected to have higher level of errors. The potential of the model in soil moisture estimation application is demonstrated by comparing nominal (global) parameterizations and optimized parameters for each field campaign. The algorithm introduced in this paper is designed to allow retrievals of surface soil moisture without any ancillary information on vegetation and roughness, two critical and problematic effects on radar backscatter. Ancillary information on these two effects is not directly indicative of L-band radar backscatter behavior. Therefore, they are a major source of uncertainty. In using simple relationships and global (nominal) parameters, there is a tradeoff in errors due to simplifications and errors due to reliance on indirect ancillary information. Several earlier approaches, including those developed for frequencies other than L-band, have reported to have soil moisture estimation accuracy comparable to those found in this paper. However, the impact of the advantages of SMAP-like radar compared with other radar sensors (such as the more sensitive L-band, more frequent revisit, and regular spatial sampling for global coverage) has not been explored yet. This paper introduces a research approach, and therefore, it is not intended to compare the accuracy level of other radar soil moisture models.

In its present form, the radar-only approach presented in this paper is deficient in several ways. It does not accurately account for effects such as terrain and vegetation morphology. The present model is intentionally simplified to begin the exploration of the path forward to radar measurement-only surface soil moisture retrieval using new L-band radar observations, such as SMAP. Given the complexity of surface effects and interactions, larger errors are expected in surface soil moisture retrievals when compared to L-band radiometer-based retrievals. The relative advantage of radar is resolution at the cost of accuracy but may still may be advantageous for many applications.

Appendix A
Soil Texture Effect on Model Parameters

In this appendix, the treatment of the soil texture effect on the model parameters is outlined. The data cube based on [29] is used to develop a parameterization [8], [14]. The data cubes have the soil dielectric constant ε as a dimension. The algorithm developed in this paper is in terms of volumetric soil moisture m_v. We use the Mironov dielectric model [38] to convert ε to m_v. The Mironov model uses information on clay fraction (clf) to account for soil texture effect.

Fig. 11 shows the effect of soil texture (captured by clf) on *Sensitivity* (S_s) and *Intercept* (σ^s_{PP}) for VV or HH polarizations and for bare soils. We use quadratic equations to account for the effects shown in Fig. 11. The resulting fits are

$$\begin{aligned} S_s(clf) &= -6.36 * clf^2 + 13.05 * clf + S0 \\ \sigma^s_{VV}(clf) &= 3.67 * clf^2 - 11.70 * clf + \sigma^{s0}_{VV} \\ \sigma^s_{HH}(clf) &= 1.64 * clf^2 - 5.71 * clf + \sigma^{s0}_{HH} \end{aligned} \tag{A1}$$

where $S0 = 20.64$, $\sigma^{s0}_{VV} = -32.30$, and $\sigma^{s0}_{HH} = -29.32$.

Acknowledgment

The authors would like to thank N. Das, A. Colliander, and S. Chan at the Jet Propulsion Laboratory, T. Jackson, M. Cosh, and R. Bindlish at the U.S. Department of Agriculture, and P. O'Neill and A. Joseph at the NASA Goddard Space Flight Center for providing data sets and advice. The authors would also like to thank D. Leroux for her help with processing the SMAPVEX12 data.

REFERENCES

[1] D. Entekhabi *et al.*, "The Soil Moisture Active and Passive (SMAP) mission," *Proc. IEEE*, vol. 98, no. 5, pp. 704–716, 2010.

[2] F. T. Ulaby, A. K. Moore, and A. K. Fung, *Microwave Remote Sensing: Active and Passive*, vol. 3, Norwood, MA, USA: Artech House, 1986.

[3] L. Tsang and J. A. Kong, *Scattering of Electromagnetic Waves*, vol. 3 Advanced Topics, Hoboken, NJ, USA: Wiley Interscience, 2001.

[4] A. K. Fung, Z. Li, and K. S. Chen, "Backscatterig from a randomly rough dielectric surface," *IEEE Trans. Geosci. Remote Sens.*, vol. 30, no. 2, pp. 356–369, Mar. 1992.

[5] Y. Oh, K. Sarabandi, and F. T. Ulaby, "An empirical model and an inversion technique for radar scattering from bare soil surfaces," *IEEE Trans. Geosci. Remote Sens.*, vol. 30, no. 2, pp. 370–381, Mar. 1992.

[6] P. C. Dubois, J. van Zyl, and T. Engman, "Measuring soil moisture with imaging radars," *IEEE Trans. Geosci. Remote Sens.*, vol. 33, no. 4, pp. 915–926, Jul. 1995.

[7] J. Shi, J. Wang, A. Y. Hsu, P. E. O'Neill, and E. T. Engman, "Estimation of bare surface soil moisture and surface roughness parameter using L-band SAR image data," *IEEE Trans. Geosci. Remote Sens.*, vol. 35, no. 5, pp. 1254–1266, Sep. 1997.

[8] S. Kim *et al.*, "L-band radar backscatter coefficients models over the global terrain for soil moisture retrieval," *IEEE Trans. Geosci. Remote Sens.*, vol. 52, no. 2, pp. 1381–1396, 2014, 2012.

[9] R. Bindlish and A. P. Barros, "Parameterization of vegetation backscatter in radar-based soil moisture estimation," *Remote Sens.Environ.*, vol. 76, no. 1, pp. 130–137, 2001.

[10] Y. Oh, "Quantitative retrieval of soil moisture content and surface roughness from multipolarized radar observations of bare soil surfaces," *IEEE Trans. Geosci. Remote Sens.*, vol. 42, no. 3, pp. 596–601, Mar. 2004.

[11] E. Njoku *et al.*, "Observations of soil moisture using a passive and active low frequency microwave airborne sensor during SGP99," *IEEE Trans. Geosci. Remote Sens.*, vol. 40, no. 12, pp. 2659–2673, Dec. 2002.

[12] U. Narayan, V. Lakshmi, and T. J. Jackson, "High-resolution change estimation of soil moisture using L-band radiometer and radar observations made during the SMEX02 experiments," *IEEE Trans. Geosci. Remote Sens.*, vol. 44, no. 6, pp. 1545–1554, Jun. 2006.

[13] Y. Kim and J. J. van Zyl, "A time-series approach to estimate soil moisture using polarimetric radar data," *IEEE Trans. Geosci. Remote Sens.*, vol. 47, no. 8, pp. 2519–2527, Aug. 2009.

[14] S. Kim *et al.*, "Soil moisture retrieval using time-series radar observations over bare surfaces," *IEEE Trans. Geosci. Remote Sens.*, vol. 50, no. 5, pp. 1853–1863, May 2012.

[15] W. Wagner and K. Scipal, "Large-scale soil moisture mapping in western Africa using the ERS scatterometer," *IEEE Trans. Geosci. Remote Sens.*, vol. 38, no. 4, pp. 1777–1782, Jul. 2000.

[16] D. Roo, Y. Du, F. Ulaby, and C. Dobson, "A semi-empirical backscattering model at L-band and C-band for a soybean canopy with soil moisture inversion" *IEEE Trans. Geosci. Remote Sens.*, vol. 39, no. 4, pp. 864–872, Apr. 2001.

[17] M. Zribi and M. Dechambre, "A new empirical model to retrieve soil moisture and roughness from C-band radar data," *Remote Sens. Environ.*, vol. 84, no. 1, pp. 42–52, Jan. 2002.

[18] F. Mattia, G. Satalino, L. Dente and G. Pasquariello, "Using a priori information to improve soil moisture retrieval from ENVISAT ASAR AP data in semiarid regions," *IEEE Trans. Geosci. Remote Sens.*, vol. 44, no. 4, pp. 900–912, Apr. 2006.

[19] A. Joseph, R. van der Velde, P. O'Neill, R. Lang, and T. Gish, "Using a priori information to improve soil moisture retrieval from ENVISAT ASAR AP data in semiarid regions," *IEEE Trans. Geosci. Remote Sens.*, vol. 46, no. 8, pp. 2365–2374, Aug. 2008.

[20] S. Paloscia, P. Pampaloni, S. Pettinato, and E. Santi, "A comparison of algorithms for retrieving soil moisture from ENVISAT/ASAR images," *IEEE Trans. Geosci. Remote Sens.*, vol. 46, no. 10, pp. 3274–3284, Oct. 2008.

[21] M. Zribi, C. André, and B. Decharme, "A method for soil moisture estimation in Western Africa based on the ERS scatterometer," *IEEE Trans. Geosci. Remote Sens.*, vol. 46, no. 2, pp. 438–448, Feb. 2008.

[22] N. Baghdadi, J. Chaaya, and M. Zribi, "Semiempirical calibration of the integral equation model for SAR data in C-band and cross polarization using radar images and field measurements," *IEEE Geosci. Remote Sens. Lett.*, vol. 8, no. 1, pp. 14–18, Jan. 2011.

[23] A. Balenzano, F. Mattia, G. Satalino, and M. Davidson, "Dense temporal series of C- and L-band SAR data for soil moisture retrieval over agricultural crops," *IEEE J. Sel. Topics Appl. Earth Observ. Remote Sens.*, vol. 4, no. 2, pp. 439–450, Jun. 2011.

[24] H. Lievens and N. E. C. Verhoest, "On the retrieval of soil moisture in wheat fields from L-band SAR based on water cloud modeling, the IEM, and effective roughness parameters," *IEEE Geosci. Remote Sens. Lett.*, vol. 8, no. 4, pp. 740–744, Jul. 2011.

[25] N. Baghdadi, M. Aubert, and M. Zribi, "Use of TerraSAR-X data to retrieve soil moisture over bare soil agricultural fields," *IEEE Geosci. Remote Sens. Lett.*, vol. 9, no. 3, pp. 512–516, May 2012.

[26] SMAP project, "SMAP Algorithm Theoretical Basis Document: L2 & L3 Radar Soil Moisture (Passive) Products: http://smap.jpl.nasa.gov/science/dataproducts/ATBD/

[27] S. Yueh *et al.*, "Passive and active L-band system and observations during the 2007 CLASIC campaign," in *Proc. IEEE Int. Geosci. Remote Sens. Symp.*, Boston, MA, USA, 2008, pp. II-241–II-244.

[28] Y. Kim, T. Jackson, R. Bindlish, H. Lee, and S. Hong, "Radar vegetation index for estimating the vegetation water content of rice and soybean," *IEEE Geosci. Remote Sens. Lett.*, vol. 9, no. 4, pp. 564–568, Jul. 2012.

[29] S. W. Huang, L. Tsang, E. Njoku, and K. S. Chen, "Backscattering coefficients, coherent reflectivities, and emissivities of randomly rough soil surfaces at L-band for SMAP applications based on numerical solutions of Maxwell equations in 3-D simulations," *IEEE Trans. Geosci. Remote. Sens.*, vol. 48, no. 6, pp. 2557–2568, Jun. 2010.

[30] A. Colliander *et al.*, "Long term analysis of PALS soil moisture campaign measurements for global soil moisture algorithm development," *Remote Sens. Environ.*, vol. 121, pp. 309–322, Jun. 2012.

[31] H. McNairn *et al.*, "The Soil Moisture Active Passive Validation Experiment 2012 (SMAPVEX12): Prelaunch calibration and validation of the SMAP soil moisture algorithms," *IEEE Trans. Geosci. Remote Sens.*, vol. 53, no. 5, pp. 2784–2801, May 2015.

[32] Y. Du, F. T. Ulaby, and M. C. Dobson, "Sensitivity to soil moisture by active and passive microwave sensors," *IEEE Trans. Geosci. Remote Sens.*, vol. 38, no. 1, pp. 105–113, Jan. 2000.

[33] J. R. Wang, E. T. Engman, T. J. Schmugge, T. Mo and J. C. Shiue, "The effects of soil moisture, surface roughness, and vegetation on L-band emission and backscatter," *IEEE Trans. Geosci. Remote Sens.*, vol. GE-25, no. 6, pp. 825–833, Nov. 1987.

[34] M. Aubert *et al.*, "Analysis of TerraSAR-X data sensitivity to bare soil moisture, roughness, composition and soil crust," *Remote Sens. Environ.*, vol. 115, no. 8, pp. 1801–1810, Aug. 2011.

[35] F. T. Ulaby and P. P. Batliwala, "Optimum radar parameters for mapping soil moisture," *IEEE Trans. Geosci. Electron.*, vol. GE-14, no. 2, pp. 81–93, Apr. 1976.

[36] M. Burgin, D. Clewley, R. Lucas, and M. Moghaddam, A generalized radar backscattering model based on wave theory for multilayer multispecies vegetation. *IEEE Trans. Geosci. Remote Sens.*, 49, no. 12, pp. 4832–4845, Dec. 2011.

[37] M. Arii, J. J. van Zyl, and Y. Kim, "A general characterization for polarimetric scattering from vegetation canopies," *IEEE Trans. Geosci. Remote Sens.*, vol. 48, no. 9, pp. 3349–3357, Sep. 2010.

[38] V. L. Mironov, M. C. Dobson, V. H. Kaupp, S. A. Komarov, and V. N. Kleshchenko, "Generalized refractive mixing dielectric model for moist soil," *IEEE Trans. Geosci. Remote Sens.*, vol. 42, no. 4, pp. 773–785, Apr. 2004.

[39] K. S. Chen and A. K. Fung, "A comparison of backscattering models for rough surfaces," *IEEE Trans. Geosci. Remote Sens.*, vol. 33, no. 1, pp. 195–200, Jan. 1995.

[40] Q. Li, J. Shi, and K. S. Chen, "A generalized power law spectrum and its applications to the backscattering of soil surface based on the integral equation model," *IEEE Trans. Geosci. Remote Sens.*, vol. 40, no. 2, pp. 271–290, Feb. 2002.

[41] A. Loew and W. Mauser, "A semiempirical surface backscattering model for bare soil surfaces based on a generalized power law spectrum approach," *IEEE Trans. Geosci. Remote Sens.*, vol. 44, no. 4, pp. 1022–1035, Apr. 2006.

[42] M. M. Rahman *et al.*, "A derivation of roughness correlation length for parameterizing radar backscatter models," *Int. J. Remote Sens.*, vol. 28, no. 18, pp. 3995–4012, 2007.

[43] J. P. Wigneron, P. Ferrazzoli, A. Olioso, P. Bertuzii, and A. Chanzy, "A simple approach to monitor crop biomass from C-band radar data," *Remote Sens. Environ.*, vol. 69, pp. 179–188, 1999.

[44] Y. Oh, K. Sarabandi, and F. T. Ulaby, "Semi-empirical model of the ensemble-averaged differential Mueller matrix for microwave backscattering from bare soil surfaces," *IEEE Trans. Geosci. Remote Sensing*, vol. 40, no. 6, pp. 1348–1355, Jun. 2002.

[45] I. Hajnsek, E. Pottier, and S. Cloude, "Inversion of surface parameters from polarimetric SAR," *IEEE Trans. Geosci. Remote Sens.*, vol. 41, no. 4, pp. 727–744, Apr. 2003.

[46] D. Entekhabi, R. H. Reichle, R. D. Koster, and W. T. Crow, "Performance metrics for soil moisture retrievals and application requirements," *J. Hydrometeor.*, vol. 11, no. 3, pp. 832–840, Jun. 2010.
[47] R. Bindlish *et al.*, "Combined passive and active microwave observations of soil moisture during CLASIC," *IEEE Geosci. Remote Sens. Lett.*, vol. 6, no. 4, pp. 644–648, Oct. 2009.
[48] U. K. Khankhoje, J. J. van Zyl, and T. A. Cwik, "Computation of radar scattering from heterogeneous rough soil using the finite-element method," *IEEE Trans. Geosci. Remote Sens.*, vol. 51, no. 6, pp. 3461–3469, Jun. 2013.
[49] J. Boisvert *et al.*, "Effect of surface soil moisture gradients on modelling radar backscattering from bare fields," *Int. J. Remote Sens.*, vol. 18, no. 1, pp. 153–170, Jan. 1997.
[50] N. Pierdicaa, L. Pulvirenti and C. Bignami, "Soil moisture estimation over vegetated terrains using multitemporal remote sensing data," *Remote Sens. Environ.*, vol. 114, pp. 440–448, 2010.

Parag S. Narvekar (M'13) received the Ph.D. degree in polarimetric microwave remote sensing of land and snow/ice from the University of Bremen, Bremen, Germany, in 2007.

Since 2011, he has been with the Massachusetts Institute of Technology, Cambridge, MA, USA. During 2011–2014, he was also jointly appointed at the Jet Propulsion Laboratory, CA, USA, as a Research Affiliate. Earlier, he worked at different institutes, including the U.S. Department of Agriculture in Maryland, USA, the City University of New York, New York, NY, USA, the University of Bremen, and the Indian Institute of Technology Bombay, India. He has served on the NASA and National Science Foundation grant review panels and is a recipient of the Massachusetts Institute of Technology "Big Data" educational fellowship. His research interest primarily includes the application and development of remote sensing technology for estimating land surface geophysical quantities in real time needed in a variety of agricultural and hydrological applications.

Dara Entekhabi (M'04–SM'09) received the B.S. and M.S. degrees from Clark University, Worcester, MA, USA, and the Ph.D. degree from the Massachusetts Institute of Technology (MIT), Cambridge, MA, USA, in 1990.

He is currently a Professor with the Department of Civil and Environmental Engineering and the Department of Earth, Atmospheric and Planetary Sciences at MIT. He is the Lead of the Science Team for the National Aeronautics and Space Administration's Soil Moisture Active and Passive (SMAP) mission, to be launched in January 2015. His research work includes terrestrial remote sensing, data assimilation, and coupled land-atmosphere systems modeling.

Dr. Entekhabi is a Fellow of the American Meteorological Society and the American Geophysical Union.

Seung-Bum Kim received the B.Sc. degree in electrical engineering from the Korea Advanced Institute of Science and Technology (KAIST), Daejeon, Korea, in 1992 and the M.S. and Ph.D. degrees in remote sensing from the University College London, U.K., in 1993 and 1998, respectively.

He has worked on spaceborne photogrammetry to generate land topography with SPOT images and microwave radiometry with AMSR-E data in KAIST until 2003. He conducted ocean science research of mixed-layer dynamics in the Jet Propulsion Laboratory until 2006. He was a Scientist at Remote Sensing Systems, CA, USA, studying L-band radiometry for the Aquarius salinity observation. He has been with the Jet Propulsion Laboratory since 2009. His current research includes microwave modeling, soil moisture retrieval with radar data from the Soil Moisture Active Passive mission, and salinity retrieval with Aquarius data. He is a member of the Aquarius science team.

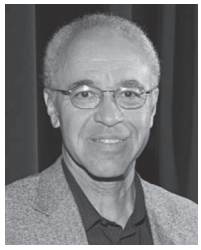

Eni G. Njoku (M'75–SM'83–F'95) received the B.A. degree in natural and electrical sciences from Cambridge University, Cambridge, U.K., in 1972 and the M.S. and Ph.D. degrees in electrical engineering from the Massachusetts Institute of Technology, Cambridge, MA, USA, in 1974 and 1976, respectively.

He is currently a Senior Research Scientist and Supervisor of the Water and Carbon Cycles Group at the Jet Propulsion Laboratory, California Institute of Technology, Pasadena, CA, USA. His research interests are in passive and active microwave sensing of soil moisture for hydrology and ecosystem applications. He was recently a Project Scientist of the Soil Moisture Active Passive mission and is a member of the U.S. Advanced Microwave Scanning Radiometer science team.

Dr. Njoku is a recipient of the NASA Exceptional Service Medal.